Three-dimensional Optical Coherence Tomography Imaging of Retinal Sheet Implants in Live Rats

Magdalene J. Seiler[1,#], **Bin Rao**[2,3,#,*], **Robert B. Aramant**[1], **Lingfeng Yu**[2], **Qiang Wang**[2], **Eric Kitayama**[1,2], **Sylvia Pham**[2], **Fengrong Yan**[1], **Zhongping Chen**[2,3], and **Hans S. Keirstead**[1]

[1] Reeve-Irvine Research Center, Sue and Bill Gross Stem Cell Research Center, Dept. Anatomy & Neurobiology, University of California, Irvine, CA

[2] Dept. Biomedical Engineering, Beckman Laser Institute, University of California, Irvine, CA

[3] Dept. Electrical Engineering & Computer Science, University of California, Irvine, CA

Abstract

Purpose—To obtain three-dimensional images from retinal transplants in live animals and evaluate the placement and structural quality of the transplants.

Methods—Donor retinal sheets were isolated from E19 fetuses of transgenic rats expressing human alkaline phosphatase (hPAP), and transplanted to the subretinal space of 19–56 d old S334ter-3 rat recipients with fast retinal degeneration (average age at surgery 32d). A total of 143 rats were imaged 1 day – 2.8 months after surgery, using a Fourier domain optical coherence tomography (FDOCT) system, with an axial resolution of 3.5 micron. The CCD A-line integration time was set at 200 μs for better visualization of degenerated retina. After targeting the transplant area, 139 or 199 consecutive slices were scanned. Projection images and movies of the retinal transplant area were computed and later compared with histology.

Results—OCT scans identified 137 of 141 transplants as a thickening of the degenerated retina. OCT indicated the laminar structure of the transplants and surgical defects, such as RPE/choroid damage with an accuracy rate between 83 and 99%. Three-dimensional projections showed the transplant position in the retina in relation to the optic disc. Histology of transplants by hPAP and hematoxylin-eosin staining was correlated with the OCT results.

Conclusions—Optical Coherence Tomography is an excellent tool to image retinal layers in a live rat. This procedure helps to evaluate the placement and quality of the transplants in the living eye.

Corresponding author: Hans S. Keirstead, Associate Professor of Anatomy and Neurobiology, Co-Director of the Sue and Bill Gross Stem Cell Research Center, Reeve-Irvine Research Center, Sue and Bill Gross Stem Cell Research Center, 2111 Gillespie Neuroscience Research Facility, School of Medicine, University of California at Irvine, Irvine, CA, 92697-4292, Phone: (949) 824-6213, Fax: (949) 824-5352, hansk@uci.edu.

Co-corresponding author (for imaging): Zhongping Chen, Associate Professor of Biomedical Engineering, University of California, Irvine, Biomedical Engineering, Beckman Research Center, 1002 Health Sciences Road E, Irvine, CA 92697-1475, Phone: (949) 824-1247, Fax: (949) 824-8413

[#]Both authors contributed equally to the manuscript.

[*]Bin Rao's current address is at the Department of Biomedical Engineering, Washington University, St. Louis, MO.

Keywords

Retinal imaging; Fourier-domain; laser; retinal degeneration; retinal transplantation; human placental alkaline phosphatase

Introduction

Transplantation of retinal sheets (review: Aramant and Seiler, 2004; Seiler and Aramant, 2005) aims at replacing photoreceptors and/or retinal pigment epithelium (RPE) (and other retinal cells) lost in retinal diseases such as age-related macular degeneration (AMD) or retinitis pigmentosa (RP). AMD is the leading cause of blindness among the elderly, affecting about 8 million patients in the U.S. alone (Ding et al., 2009; Jager et al., 2008), and retinitis pigmentosa is an inherited disease that affects about a million patients worldwide (Kennan et al., 2005). The inner retina remains still functional for the some time after photoreceptor loss (Humayun et al., 1999), so it may be possible to restore visual function if newly replaced retinal cells can connect with the remaining host circuitry. Using a special implantation instrument, it has been possible to gently transplant sheets of fetal retina to the subretinal space in rodent retinal degeneration models (Aramant and Seiler, 2004; Seiler and Aramant, 2005) and in human patients (Radtke et al., 2008).

The surgery in the small rat eye is however very challenging since the surgeon cannot observe where the tissue is placed. Only about 20–30% of all transplants develop a normal lamination with photoreceptor outer segments facing the host RPE, in contrast to balls of photoreceptors in rosettes (Seiler and Aramant, 1998). It is very difficult to judge the quality of transplants in fundus exams due to the transparency of the transplant and host retina. To save resources, it would be important to eliminate transplanted rats with surgical defects early on from the study. Therefore, we developed a systematic approach to evaluate transplants in live rats by three-dimensional ocular coherence tomography (OCT) which provides a means to analyze structures in the living eye (Jeon et al., 2008b).

In contrast to a previous study (Thomas et al., 2006) that used a commercially available time domain Zeiss Stratus OCT, the OCT setup for this study used serial scans of a Fourier Domain OCT to provide a three-dimensional image of the transplant in the eye (Jeon et al., 2008a; Leitgeb et al., 2003; Zhang et al., 2004). The purpose of this study was to evaluate the accuracy of the 3D-FDOCT to predict later histological results.

Materials and Methods

Animals

For all experimental procedures, animals were treated in accordance with the NIH guidelines for the care and use of laboratory animals and the ARVO Statement for the Use of Animals in Ophthalmic and Vision Research, under a protocol approved by the Institutional Animal Care and Use Committee of the University of California, Irvine. Pigmented S334ter-line-3 rats (Liu et al., 1999; Sagdullaev et al., 2003; Seiler et al., 2008a) with fast retinal degeneration were used in this study. The rats were originally produced by Xenogen Biosciences (formerly Chrysalis DNX Transgenic Sciences, Princeton, NJ), and developed and supplied with the support of the National Eye Institute by Dr. Matthew LaVail, University of California San Francisco (http://www.ucsfeye.net/mlavailRDratmodels.shtml). Recipients were the F1 generation of a cross between albino homozygous S334ter-line 3 and pigmented Copenhagen rats (Harlan, Indianapolis, IN).

A total of 143 rats that had received embryonic day (E) 18–20 fetal retinal sheet transplants (n = 141) or sham surgery (n = 2) at the age of 19–56 days (average 31.9 ± 6.8 days) were evaluated with three-dimensional optical coherence tomography at the age of 26–116 days, 1 to 85 days after surgery. The donor retinal sheets were derived from transgenic hPAP (human placental alkaline phosphatase) expressing rats (Kisseberth et al., 1999). Fetal retinas were dissected free from surrounding tissues, and stored overnight in Hibernate E medium (Brainbits, IL) on ice or in the refrigerator. Some donor retinas were coated with glial-derived neurotrophic factor (GDNF) or brain-derived neurotrophic factor (BDNF) containing microspheres before transplantation (Seiler et al., 2008a) to improve the functional effect of the transplants. Immediately before transplantation, the tissue was cut to a rectangular square (about 1 mm^2) and loaded into the flat nozzle of a custom-made implantation tool (Aramant and Seiler, 2002). For the transplant surgery, recipient rats were anesthetized with Ketamine/Xylazine (K: 37.5mg/kg; X:5 mg/kg i.p), the pupils were dilated with 2% atropine, and the non-surgery eye covered with artificial tears ointment. A cut was made through sclera, choroid and retina in the periphery of the superior eyeball. The instrument nozzle was inserted into the subretinal space, advanced towards the central retina where the donor tissue was placed into the subretinal space and the nozzle withdrawn. The lesion was closed with 10-0 sutures. The transplant placement was evaluated by an eye exam following surgery. Rats with too much trauma were discontinued from the study. Rats were placed into an incubator for recovery after surgery, and surgery eyes treated with gentamycin ophthalmic ointment.

High Performance Fourier-domain Optical Coherence Tomography for Retinal Imaging

Figure 1 shows a diagram of the high performance Fourier-domain ophthalmic optical coherence tomography instrument for in vivo retinal imaging designed and built at Beckman Laser Institute (Rao et al., 2008) with an axial resolution of 3.5 μm (in adult normal rat retina), sensitivity of 106 dB and imaging speed of 5 K A lines per second. However, in the retinal degenerate rats of different ages used in this study, the resolution was likely less than 3.5 μm. The axial resolution in rat retinas of different ages was not measured. Low coherence light with a center wavelength of 890nm and FWHM bandwidth of 150 nm was protected from optical feedback using a broadband optical isolator before entering a 2 × 2 broadband fiber coupler based interferometer. The light from the reference arm was focused onto a reference mirror with an optical attenuator inserted into the optical path. The sample arm was modified from the patient module of a Zeiss© Stratus OCT instrument.

The system maintains sensitivity of 100 dB within 500 μm imaging depth range. The sensitivity roll-off over 2 mm depth range is 9 dB. The lateral resolution in the eye is 20 μm. Each scan resulted in 199 or 139 slices.

Two customized imaging modes were developed for the eye alignment. The first imaging mode is cross-scan mode. It includes both horizontal and vertical scans in a single scan and displays the real time processed image in two B-mode images. When the animal eye is positioned appropriately, both the horizontal and vertical images are not tiled on the image. The second one is fast fundus imaging mode. In this fast fundus imaging mode, a band-pass filtering of K space spectrum generates a fundus projection image without time-consuming fast Fourier transforms (FFT) that is normally used to generate the OCT image. The cross-scan mode is more efficient in finding the initial eye alignment position. The fast fundus imaging mode can be used to find the transplant's position relative to the optical nerve head.

Non-invasive Optical Coherence Tomography Imaging Procedures

Rats were imaged 1 day –2.8 months after surgery (age 0.9–3.9 months), most of them at 1 month after surgery (average age of 2–3 months). When the project was initially set up, we imaged the first set of transplanted rats almost 3 months after surgery. Then, we experimented

with different shorter times after surgery because we wanted to obtain information about transplant quality as early as possible. We determined that we needed to wait with imaging at least 2–3 weeks after transplantation to obtain good images (data not shown). Therefore, in later experiments, rats were usually imaged 3–4 weeks after transplantation. When surgical defects were found (such as choroid damage, retinal detachment), rats were sacrificed soon after analyzing the imaging results; otherwise, rats were allowed to survive for many months after surgery.

Rats were anesthetized by Ketamine/Xylazine (K: 37.5mg/kg; X: 5 mg/kg i.p.); injections were repeated if necessary after 20–30 minutes. Atropine sulfate (2%, 1 drop per eye) was applied on the cornea 5 minutes before OCT imaging procedure for pupil dilation. Artificial tears ointment was applied to the non-surgery eye, and artificial tears eye drops were frequently applied to the surgery eye during imaging. The rat was fixed on a plastic board that was mounted on a customized stage with three-dimensional translational and three-dimensional rotation freedom.

The eye was aligned with the cross-scan imaging mode of Fourier-domain OCT instrument (schematic diagram in Figure 1). The stage was rotated in order to adjust the eye orientation. Then it was translated in order to generate upright, non-tilted OCT scan images in both horizontal and vertical orientation. The above eye rotation and stage translation procedure often had to be repeated in order to find retinal transplants. Then, a full 3D scan was performed in about 40 seconds with 200µs of A-line integration time for higher signal-to-noise ratio. The 3D scan area was 2.5 by 2.5 mm, assuming the distance to the rat eye 8 mm. Each slice had 512 or 1024 A-lines for lateral scans and 700 pixels for the axial depth direction, creating an image of 512 or 1024 pixels by 700 pixels. Along depth direction, each pixel represented 4.2 µm in retinal tissue with a refractive index of 1.38. A total of 199 or 139 slices were acquired for one 3D scan with a separation of 12.5 µm between two neighboring slices. Forty-two rats were imaged at a resolution of 1024 with 199 slices, 21 rats were scanned at a resolution of 512 with 199 slices, and 80 rats were imaged at a resolution of 1024 with 139 slices. To identify the transplant location relative to the optic nerve head, at least one additional scan was performed in most cases that included both the retinal transplant and the optical nerve head. Each scan took about 5 minutes to perform except when there were complications, such as insufficient pupil dilation, corneal damage, or transplant placement far away from the optic disc. Rats were recovered in an incubator, and their eyes covered with artificial tears ointment.

Histology

Rats were either perfused through the ascending aorta with 4% paraformaldehyde in 0.1 M Na-phosphate buffer (sometimes with 0.1–0.4% glutaraldehyde added), or eye cups were immersion fixed in 4% paraformaldehyde. Eye cups were dissected and either embedded in 4% agarose for vibratome sectioning (20 experiments), or infiltrated with 30% sucrose, frozen and cut on a cryostat (123 experiments). Some vibratome sections were subsequently cut on a cryostat. Selected sections were stained with Hematoxylin-Eosin or by histochemistry for human placental alkaline phosphatase (hPAP) to identify the donor tissue in the host. Sections were incubated in hPAP substrate buffer (0.1 M Tris, 0.1M NaCl, 5 mM MgCl2, pH 9.5) for one hour at 65 °C. This inactivated rat alkaline phosphatase. hPAP was then detected by incubation with BCIP substrate solution (Sigma, St. Louis, MO) for 15–30 minutes. Selected sections were photographed using a Nikon FXA microscope equipped with a SPOT digital camera (Diagnostic Instruments, Sterling Heights, MI).

Evaluation of Retinal Transplant OCT Images and Histology

Using noncommercial computer software developed at the Beckman Laser Institute, raw OCT data were converted into image slices and three-dimensional projections were obtained from

the image data. OCT slices generated from the 3D data set of the retinal transplant were reviewed slice by slice for the evaluation of the laminated area. Evaluation of retinal transplants using OCT images was made before the availability of histology results and histology images were analyzed independently from OCT data. The OCT evaluation results were compared to the histology results reviewed from serial histology sections of the same transplant tissue.

Retinal transplants were morphologically classified into the following categories: 1) presence of a) large (>2.5 mm^2) or b) small transplant (<2.5 mm^2) or c) no transplant found. 2) Transplant organization: a) transplants with a large laminated area (transplant photoreceptors with outer segments in contact with host RPE) and some rosettes (spherical small aggregates with photoreceptors around an outer limiting membrane, inner and outer segments toward the lumen, and the inner retinal layers on the outside of the aggregates), b) transplants containing mostly rosettes with a small laminated area; and c) transplants containing rosettes only. In addition, the following surgical defects were noted: a) damage to choroid or RPE (interruption of Bruch's membrane), b) transplant extending into the vitreous (epiretinal grafts), c) optic nerve damage, and d) retinal detachment.

The efficacy of OCT evaluation was calculated from the percentage of correct classification of retinal transplants compared with the evaluation of histology results.

Results

An overview of the results is shown in Tables 1–3. OCT imaging identified most of the large transplants, but some small transplants were missed, or the transplant appeared to be smaller than the later histology results showed. Reverse mistakes were more rare (Table 1). Regarding lamination, the overall accuracy rate to identify laminated areas in the transplants were 87%. In 9% of the experiments, a laminated area was identified in OCT scans, which was later not found in sections (Table 2). RPE/choroid damage was found in 53% of the experiments by histology, mostly a small area at the edge of the transplants, but only in 41% of experiments by OCT. Transplants extending into the epiretinal space were mostly found close to the insertion site, far away from the optic disk, and therefore often missed by OCT (only 10 found by OCT; 19 were found by histology). In 6 of the experiments, optic nerve damage was identified by histology, but only in 3 experiments by OCT. Retinal detachment was identified in 9 of 10 cases (Table 3).

Figure 2 shows an example of a transplant with large lamination area; Figure 3 shows an examples of a transplants with rosettes extending through the host retina into the vitreous, and Figures 4 and 5 show examples of surgical defects (RPE/choroid damage and retinal detachment). The retinal fundus projections images (shown in Figs. 2A, 3A, 4A, and 5A) indicated where the scan was taken in relation to the optic disc. However, the transplants were not seen in the fundus projection images and could only be observed in the cross-sectional scans (Figs. 2B–C, 3B–C, 4B–D, 5B–C) which showed the RPE/choroid as a single red band. From the scans, three-dimensional movies could be constructed (Fig. 2D). Histology mostly confirmed the OCT findings (Figs. 2E, 3D, 4E, 5D).

Discussion

Fourier domain 3D OCT has become more of a routine in the clinical setting (Cense et al., 2006; Chen et al., 2009; Rao et al., 2008; Srinivasan et al., 2008; Srinivasan et al., 2006b), but imaging the small rat eye is more of a challenge. The first study to image a rodent eye, published in 2001 (Li et al., 2001), could show differences in retinal thickness, but not much else. Two studies published in 2006 and 2007 showed a high resolution of retinal layers in rodents by spectral domain OCT (Ruggeri et al., 2007; Srinivasan et al., 2006a), however only in a very

small area (1–2 mm^2) surrounding the optic disk. Since retinal transplants were often placed more than 1 mm away from the optic disk, we needed to scan a larger area than standard fundus imaging, and tilt the eye in different angles in order to find the transplant. Our previous study demonstrated OCT images of retinal transplants, but this was more a "hit or miss" imaging, and the scan did not give much information about the position of the transplant in the eye (Thomas et al., 2006).

In the current study, the 3D optical coherence tomography images of retinal transplants presented morphological details of the retinal transplants that allowed a high accuracy to locate transplants in the subretinal space, and to identify retinal detachment. However, it was relatively difficult to classify between retinal transplants with laminated area and retinal transplants with mostly rosettes, and to find small areas of RPE/choroid damage. This was due to the small area visible by the OCT scan. Transplants could easily be found when they were placed close to the optic disc, but it was more difficult to find them when they were placed further way.

The development of rosettes (Aramant and Seiler, 2002) is due to the damage of host RPE or minor trauma of the donor retinal sheets by the surgery that is much more difficult to perform on rats than on human patients. Most of the time, there are many rosettes even when the laminated area exists as well. First of all, it will be difficult to identify a laminated area when the laminated area is small. Secondly, in the laminated area, the outer segments grow in contact with RPE. Since the reflectivity of outer nuclear layer is lower comparing to other retinal layers, the OCT slice images will show a relatively low reflectivity band on top of RPE. However, there is a possibility that the sub-retinal space on top of RPE might be misinterpreted as outer segment layer. The above two reasons explained that 13% of laminated transplants were missed. On the other hand, sometimes a faint scan was misinterpreted as a laminated area. The overall post-surgery retinal transplants evaluation efficacy of our high performance, three-dimensional optical coherence tomography is 87%. Compared to the previous method (Thomas et al., 2006) for retinal transplant imaging that could only reveal 62% of retinal transplants, this is a significant improvement.

Three-dimensional projections that included both retinal transplant and optic nerve head could provide additional information about the location of retinal transplants in the eye. This information could be used to guide superior colliculus response tests (Seiler et al., 2008b; Thomas et al., 2004).

The significant advantage of the 3D OCT scanning was that consecutive 199 or 139 scans could be obtained through a given area. Thus, it was easier to discriminate different structures and to judge the position of the transplant compared to the previous study of Thomas et al., 2004 where we did random single scans without information about the orientation of the eye. Although the transplant could not be seen in the 3D projection, only in the scanned slices, one could deduct the position of the transplant in relation to the optic disc by noting the slice numbers in which the transplant appeared.

However, retinal and subretinal structures did not look as focused as in studies using standard 3D OCT imaging of rodent eyes (Ruggeri et al., 2007; Srinivasan et al., 2006a), for three reasons. The first reason is that we were imaging degenerated retina mostly of young rats (100–150g) instead of normal retina of adult rats (>200g). With the same setup, we could acquire retinal images from normal adult rats that demonstrated multiple layers clearly. The second reason could be attributed to the simple strategy we used for dispersion compensation: We used rat lenses to calibrate the dispersion-caused phase change and compensate this phase change in all imaged rat retinal tissues. The last reason may be related to the 60D diopter lens we used in the instrument. It gives acceptable results in a normal size eye of adult rats. but the

limited aperture of the small size eyes of young rats reduced the NA of the condensing lens. These young rats should be imaged with a larger NA lens such as 90D in the future studies.

For now, our experimental protocol could satisfy our study purpose although the image could potentially be improved with a more elaborated dispersion compensation strategy in future studies.

A high performance optical coherence tomography system with imaging speed of 30K A-lines per second has been reported (Potsaid et al., 2008). The technology of OCT is rapidly improving with increased importance for research and clinical applications.

Acknowledgments

## Abbreviations used

FWHM	full width at half maximum spectral width
OCT	Ocular coherence tomography
NA	numerical aperture
SLD	Superluminescent diode
IP	inner plexiform layer
IN	inner nuclear layer
ON	outer nuclear layer
RPE	retinal pigment epithelium

References

Aramant RB, Seiler MJ. Progress in retinal sheet transplantation. Prog Retin Eye Res 2004;23:475–94. [PubMed: 15302347]

Aramant RB, Seiler MJ. Retinal transplantation--advantages of intact fetal sheets. Prog Retin Eye Res 2002;21:57–73. [PubMed: 11906811]

Cense B, Chen TC, Nassif N, Pierce MC, Yun SH, Park BH, Bouma BE, Tearney GJ, de Boer JF. Ultra-high speed and ultra-high resolution spectral-domain optical coherence tomography and optical Doppler tomography in ophthalmology. Bull Soc Belge Ophtalmol 2006:123–32. [PubMed: 17265794]

Chen Y, Vuong LN, Liu J, Ho J, Srinivasan VJ, Gorczynska I, Witkin AJ, Duker JS, Schuman J, Fujimoto JG. Three-dimensional ultrahigh resolution optical coherence tomography imaging of age-related macular degeneration. Opt Express 2009;17:4046–60. [PubMed: 19259245]

Ding X, Patel M, Chan CC. Molecular pathology of age-related macular degeneration. Prog Retin Eye Res 2009;28:1–18. [PubMed: 19026761]

Humayun MS, Prince M, de Juan E Jr, Barron Y, Moskowitz M, Klock IB, Milam AH. Morphometric analysis of the extramacular retina from postmortem eyes with retinitis pigmentosa. Invest Ophthalmol Vis Sci 1999;40:143–8. [PubMed: 9888437]

Jager RD, Mieler WF, Miller JW. Age-related macular degeneration. N Engl J Med 2008;358:2606–17. [PubMed: 18550876]

Jeon MY, Zhang J, Chen Z. Characterization of Fourier domain mode-locked wavelength swept laser for optical coherence tomography imaging. Opt Express 2008a;16:3727–37. [PubMed: 18542467]

Jeon MY, Zhang J, Wang Q, Chen Z. High-speed and wide bandwidth Fourier domain mode-locked wavelength swept laser with multiple SOAs. Opt Express 2008b;16:2547–54. [PubMed: 18542336]

Kennan A, Aherne A, Humphries P. Light in retinitis pigmentosa. Trends Genet 2005;21:103–10. [PubMed: 15661356]

Kisseberth WC, Brettingen NT, Lohse JK, Sandgren EP. Ubiquitous expression of marker transgenes in mice and rats. Dev Biol 1999;214:128–38. [PubMed: 10491262]

Leitgeb R, Hitzenberger C, Fercher A. Performance of fourier domain vs. time domain optical coherence tomography. Opt Express 2003;11:889–94. [PubMed: 19461802]

Li Q, Timmers AM, Hunter K, Gonzalez-Pola C, Lewin AS, Reitze DH, Hauswirth WW. Noninvasive imaging by optical coherence tomography to monitor retinal degeneration in the mouse. Invest Ophthalmol Vis Sci 2001;42:2981–9. [PubMed: 11687546]

Liu C, Li Y, Peng M, Laties AM, Wen R. Activation of caspase-3 in the retina of transgenic rats with the rhodopsin mutation s334ter during photoreceptor degeneration. J Neurosci 1999;19:4778–85. [PubMed: 10366612]

Potsaid B, Gorczynska I, Srinivasan VJ, Chen Y, Jiang J, Cable A, Fujimoto JG. Ultrahigh speed spectral/ Fourier domain OCT ophthalmic imaging at 70,000 to 312,500 axial scans per second. Opt Express 2008;16:15149–69. [PubMed: 18795054]

Radtke ND, Aramant RB, Petry HM, Green PT, Pidwell DJ, Seiler MJ. Vision Improvement in Retinal Degeneration Patients by Implantation of Retina Together with Retinal Pigment Epithelium. Am J Ophthalmol 2008;146:172–82. [PubMed: 18547537]

Rao B, Yu L, Chiang HK, Zacharias LC, Kurtz RM, Kuppermann BD, Chen Z. Imaging pulsatile retinal blood flow in human eye. J Biomed Opt 2008;13:040505. [PubMed: 19021308]

Ruggeri M, Wehbe H, Jiao S, Gregori G, Jockovich ME, Hackam A, Duan Y, Puliafito CA. In vivo three-dimensional high-resolution imaging of rodent retina with spectral-domain optical coherence tomography. Invest Ophthalmol Vis Sci 2007;48:1808–14. [PubMed: 17389515]

Sagdullaev BT, Aramant RB, Seiler MJ, Woch G, McCall MA. Retinal transplantation-induced recovery of retinotectal visual function in a rodent model of retinitis pigmentosa. Invest Ophthalmol Vis Sci 2003;44:1686–95. [PubMed: 12657610]

Seiler MJ, Aramant RB. Intact sheets of fetal retina transplanted to restore damaged rat retinas. Invest Ophthalmol Vis Sci 1998;39:2121–31. [PubMed: 9761291]

Seiler MJ, Aramant RB. Transplantation of neuroblastic progenitor cells as a sheet preserves and restores retinal function. Semin Ophthalmol 2005;20:31–42. [PubMed: 15804842]

Seiler MJ, Thomas BB, Chen Z, Arai S, Chadalavada S, Mahoney MJ, Sadda SR, Aramant RB. BDNF-treated retinal progenitor sheets transplanted to degenerate rats: improved restoration of visual function. Exp Eye Res 2008a;86:92–104. [PubMed: 17983616]

Seiler MJ, Thomas BB, Chen ZRW, Sadda SR, Aramant RB. Retinal transplants restore visual responses - Trans-synaptic tracing from visually responsive sites labels transplant neurons. Eur J Neurosci 2008b;28:208–20. [PubMed: 18662343]

Srinivasan VJ, Adler DC, Chen Y, Gorczynska I, Huber R, Duker JS, Schuman JS, Fujimoto JG. Ultrahigh-speed optical coherence tomography for three-dimensional and en face imaging of the retina and optic nerve head. Invest Ophthalmol Vis Sci 2008;49:5103–10. [PubMed: 18658089]

Srinivasan VJ, Ko TH, Wojtkowski M, Carvalho M, Clermont A, Bursell SE, Song QH, Lem J, Duker JS, Schuman JS, Fujimoto JG. Noninvasive volumetric imaging and morphometry of the rodent retina with high-speed, ultrahigh-resolution optical coherence tomography. Invest Ophthalmol Vis Sci 2006a;47:5522–8. [PubMed: 17122144]

Srinivasan VJ, Wojtkowski M, Witkin AJ, Duker JS, Ko TH, Carvalho M, Schuman JS, Kowalczyk A, Fujimoto JG. High-definition and 3-dimensional imaging of macular pathologies with high-speed ultrahigh-resolution optical coherence tomography. Ophthalmology 2006b;113:2054, e1–14. [PubMed: 17074565]

Thomas BB, Arai S, Ikai Y, Qiu G, Chen Z, Aramant RB, Sadda SR, Seiler MJ. Retinal transplants evaluated by optical coherence tomography in photoreceptor degenerate rats. J Neurosci Methods 2006;151:186–93. [PubMed: 16129495]

Thomas BB, Seiler MJ, Sadda SR, Aramant RB. Superior colliculus responses to light -preserved by transplantation in a slow degeneration rat model. Exp Eye Res 2004;79:29–39. [PubMed: 15183098]

Zhang J, Jung W, Nelson J, Chen Z. Full range polarization-sensitive Fourier domain optical coherence tomography. Opt Express 2004;12:6033–9. [PubMed: 19488244]
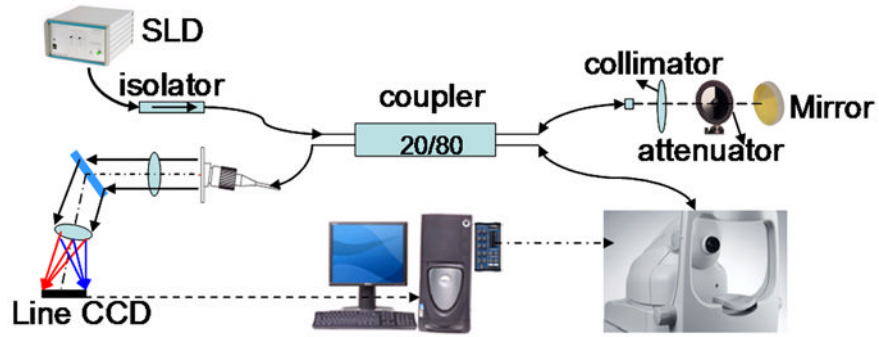
Figure 1. OCT imaging setup
The light from a Superluminescent Diode (SLD) Light Source (with the central wavelength at 890 nm and a full width at half maximum spectral width (FWHM) of 150 nm), is protected from optical feedback using a broadband optical isolator before entering a 2×2 broadband fiber coupler based interferometer. The light from the reference arm is focused onto a reference mirror with an optical attenuator inserted into the optical path. The sample arm is modified from the patient module of a Zeiss© Stratus OCT instrument. The sample information is then transferred back through a sequence of lenses and mirrors to a Line CCD camera.
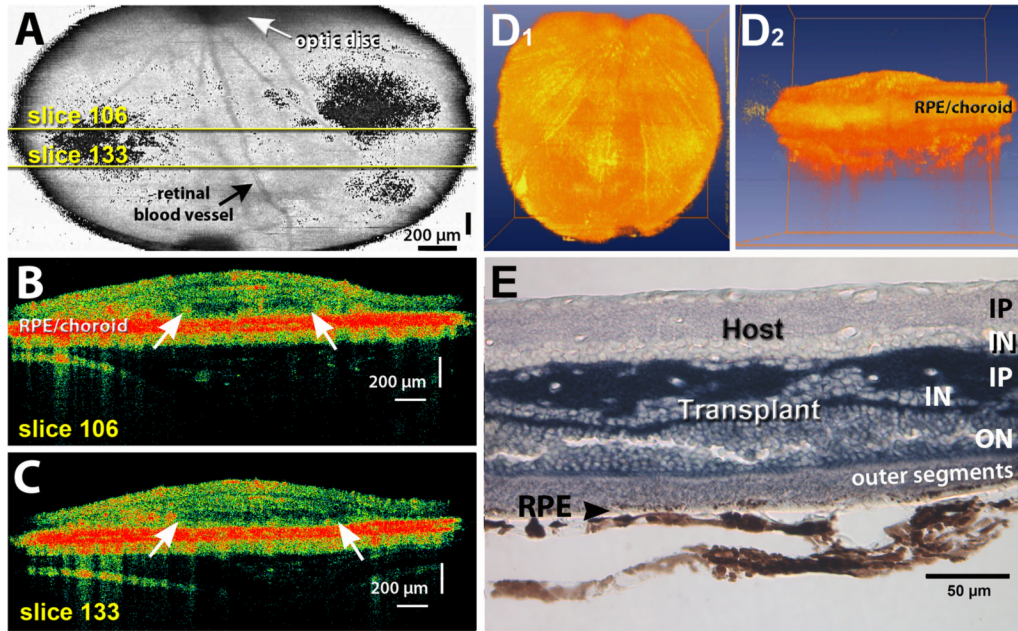
Figure 2. Example of transplant with large laminated area
A) OCT scan taken at the age of 3.6 months, 2.2 months after surgery. 3D projection of 199 OCT image slices to generate fundus image, showing which area of the eye was scanned. The transplant was recognizable on slices 39–198 of the 199 slices, but is not visible in the 3D projection. Yellow lines indicate positions of scans shown in B–C). The optic disc is recognizable on the top as a dark circle from which retinal vessels radiate out. Dark indicates strongly reflective areas (red in scan images). Size of scan area is 2.5×2.5 mm. **B), C)** Examples of OCT scan images (slice 106 and 133) of the same scan. The area between the arrows shows a clearly recognizable outer nuclear layer (appears dark), with a thin inner nuclear layer above it. The interface between host and transplant is indicated by a thin dark line. The dark red band indicates pigmented RPE and choroid. **D)** 3D rotations through scan. Movies were created using AMIRA® to represent OCT data acquired from a single scan (200 image slices). The rotating hologram shows the retinal transplant from above (D_1) and from the side (D_2). The side view shows the thickening of the retina in the transplant area above the yellow band (choroid). **E)** Histology 8.5 months after transplantation (age 9.9 months) confirms large area of lamination, with photoreceptor outer segments in contact with host RPE. Cryostat section of vibratome slice in transplant center, cytoplasm of transplant cells (without nuclei) stained dark blue for the donor marker human placental alkaline phosphatase (hPAP). Scale bars = 200 μm (A–C), 50 μm (E).
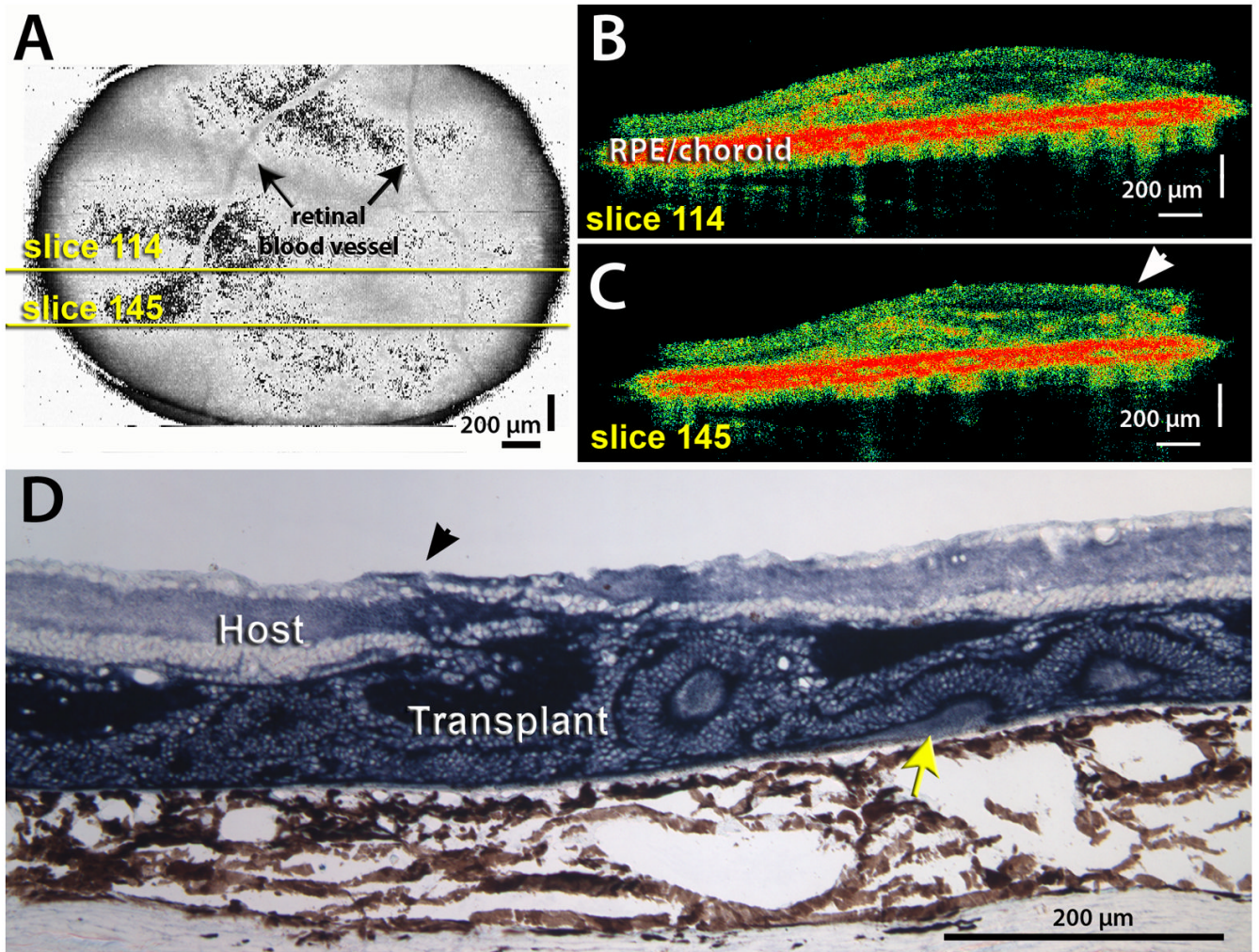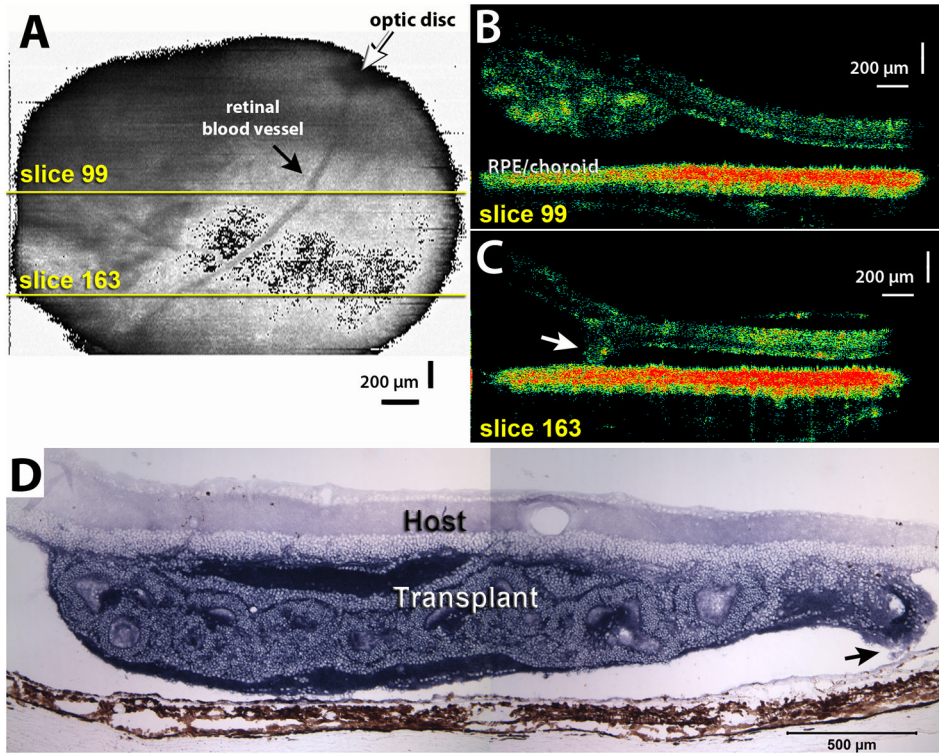
Figure 3. Example of rosetted transplant
A) Fundus projection obtained from an OCT scan of a retinal transplant area at 2.1 month post surgery, rat age 3.2 months. Yellow lines indicate positions of scans shown in B). The optic disc is outside the scan area where the blood vessels would converge. **B) C)** Examples of 2 slices through graft. Rosettes are indicated by highly reflective red dots in the OCT image; arrowhead in C) indicates an area where the transplant extends through the host retina into the vitreous. The interface between host and transplant is indicated by a thin dark line. **D)** Histology of same transplant at 2.5 months post surgery, oriented with the ganglion cell layer up and the RPE/choroid down. Transplant stained dark blue for donor hPAP marker. Arrowhead indicates penetration of transplant (blue stain) through host retina into vitreous. Most of the transplant is filled with rosettes (circular arrangement of photoreceptors). Note that a small area of correct transplant lamination with outer segments (yellow arrow) was missed in the OCT. Scale bars = 200 μm.
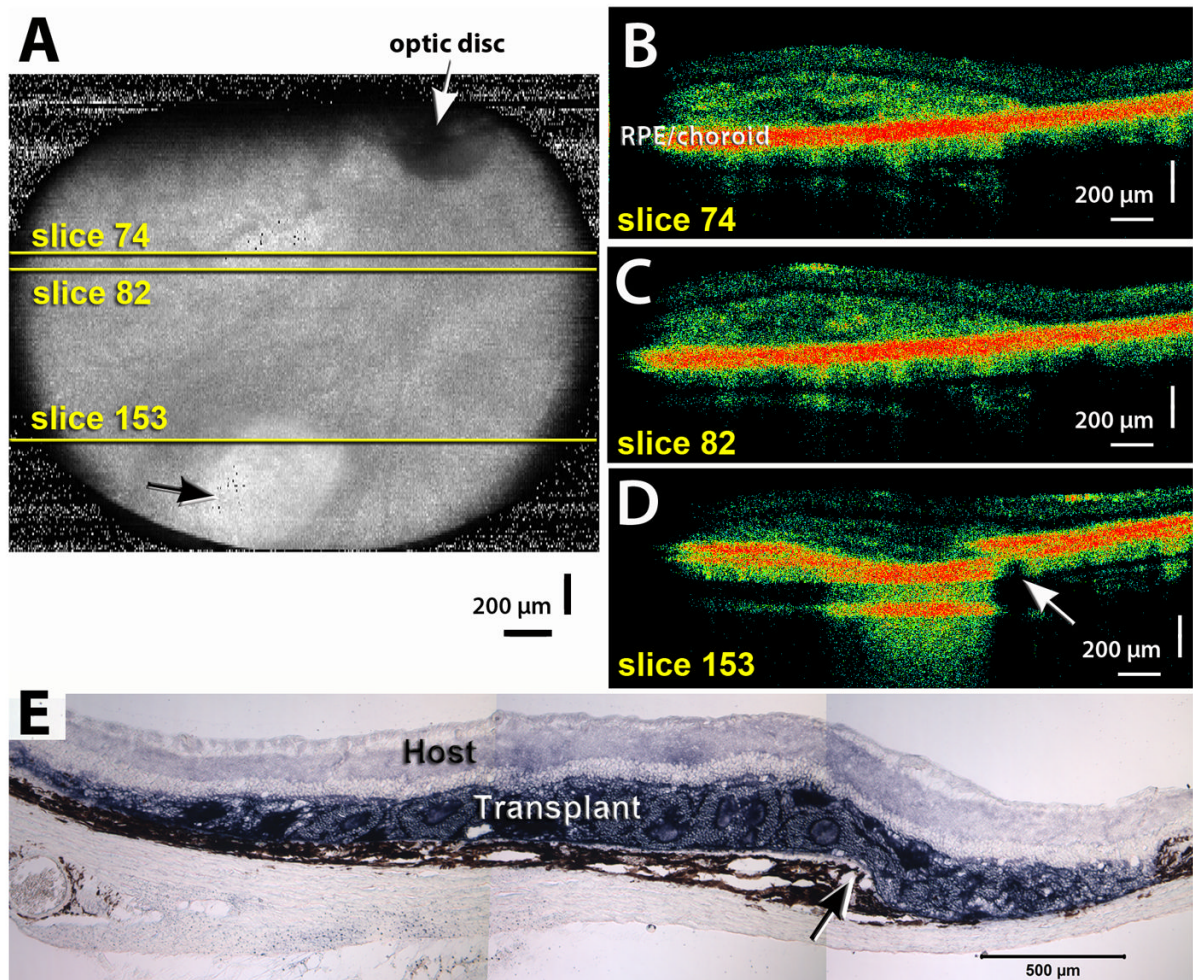
Figure 4. Example of choroid damage
A) Fundus projection obtained from an OCT scan of a retinal transplant area at 0.4 month post surgery (rat age 1.2 months). White arrow points to optic disc. Black arrow points to whitish areas, indicating choroid damage. Yellow lines indicate positions of scans shown in B–D). **B)**–**D)** Examples of 3 slices through graft. Slice 74 (B) indicates a small laminated area and rosettes, slice 82 (C) shows rosettes, and slice 153 (D) shows a break of Bruch's membrane at the edge of the transplant (arrow). **E)** Histology of same transplant at 0.9 months post surgery, showing the area with choroid damage (arrow). The choroid damage shown in this example is more severe than in most examples of choroid damage found in these experiments. Scale bars = 200 μm (A–D), 500 μm (E).

Figure 5. Example of retinal detachment
A) Fundus projection obtained from an OCT scan of a retinal transplant area at 0.9 month post surgery (rat age 1.9 months). Yellow lines indicate positions of scans shown in B–C). **B–C)** Examples of 2 slices through graft. Slice 99 (B) indicates a rosetted transplant attached to a detached host retina (black space between transplant and host RPE/choroid), slice 163 (C) shows an area where the edge of the transplant (arrow) is in contact with the host RPE. **D)** Histology of same transplant at 1 month post surgery, confirming the retinal detachment. The transplant exhibits rosettes only. Arrow indicates area where tip of transplant in attached to RPE (scan area of C). Scale bars = 200 μm (A,B), 500 μm (C).

Table 1

Comparison of OCT and histology results – Transplant size

N = 143 (= total #)	Large graft (>2.5 mm²)	Small graft (<2.5 mm²)	No graft
OCT (N)	114	23	6
OCT (% of total)	80%	16%	4%
Histology (N)	121	20	2
Histology (% of total)	85%	14%	1%

	Large graft missed	Small graft missed	Graft larger in OCT scan than in histology	Graft smaller in OCT scan than in histology	Small graft in OCT, no graft in section
Features missed by OCT	1	4	2	7	1
% mistake rate	1%	3%	1%	5%	1%
Accuracy rate	99%	97%	99%	95%	99%

Table 2

Comparison of OCT and histology results – Transplant lamination

	Laminated area	Large laminated area + rosettes[**]	Rosettes + small laminated area[***]	Rosettes only
OCT (N = 137)	66	27	39	71
OCT (% of total)	48%	20%	28%	52%
Histology (N = 141)	68	35	33	70
Histology (% of total)	48%	25%	23%	50%
	Laminated areas missed (large & small)	Large laminated area missed	Small laminated area missed	Lamination in OCT, but not in sections
Features missed by OCT	18[*]	11	14	13
% mistake rate	13%	8%	10%	9%
Accuracy rate	87%	92%	90%	91%

[*] Experiments where a lamination area was estimated too large or too small are not included.

[**] Large laminated area: lamination in most of cross-section

[***] Small laminated area: less than 30% in cross-section

N = total # of experiments minus experiments without transplant.

Table 3

Comparison of OCT and histology results – Surgical damage, transplant misplacement

N = 143	Choroid damage or RPE scar	(part of) transplant epiretinal	Optic nerve damage	Retinal detachment
OCT (N)	58	10	3	9
OCT (% of total)	41%	7%	2%	6%
Histology (N)	76	19	6	10
Histology (% of total)	53%	13%	4%	7%
Features missed by OCT	16	8	3	1
% mistake rate	21% (16/76)	42% (8/19)	50% (3/6)	10% (9/10)
Accuracy rate	79%	58%	50%	90%